EUROPEAN LABORATORY FOR PARTICLE PHYSICS

CERN-EP/99-082
14th June 1999

A Study of Spin Alignment of $\rho(770)^{\pm}$ and $\omega(782)$ Mesons in Hadronic Z^0 Decays

The OPAL Collaboration

Abstract

The helicity density matrix elements ρ_{00} of $\rho(770)^{\pm}$ and $\omega(782)$ mesons produced in Z^0 decays have been measured using the OPAL detector at LEP. Over the measured meson energy range, the values are compatible with 1/3, corresponding to a statistical mix of helicity -1, 0 and $+1$ states. For the highest accessible scaled energy range $0.3 < x_E < 0.6$, the measured ρ_{00} values of the $\rho^{\pm}$ and the ω are 0.373 ± 0.052 and 0.142 ± 0.114, respectively. These results are compared to measurements of other vector mesons.

(To be submitted to European Physical Journal C)

The OPAL Collaboration

G. Abbiendi[2], K. Ackerstaff[8], G. Alexander[23], J. Allison[16], N. Altekamp[5], K.J. Anderson[9], S. Anderson[12], S. Arcelli[17], S. Asai[24], S.F. Ashby[1], D. Axen[29], G. Azuelos[18,a], A.H. Ball[8], E. Barberio[8], R.J. Barlow[16], J.R. Batley[5], S. Baumann[3], J. Bechtluft[14], T. Behnke[27], K.W. Bell[20], G. Bella[23], A. Bellerive[9], S. Bentvelsen[8], S. Bethke[14], S. Betts[15], O. Biebel[14], A. Biguzzi[5], I.J. Bloodworth[1], P. Bock[11], J. Böhme[14], D. Bonacorsi[2], M. Boutemeur[33], S. Braibant[8], P. Bright-Thomas[1], L. Brigliadori[2], R.M. Brown[20], H.J. Burckhart[8], P. Capiluppi[2], R.K. Carnegie[6], A.A. Carter[13], J.R. Carter[5], C.Y. Chang[17], D.G. Charlton[1,b], D. Chrisman[4], C. Ciocca[2], P.E.L. Clarke[15], E. Clay[15], I. Cohen[23], J.E. Conboy[15], O.C. Cooke[8], J. Couchman[15], C. Couyoumtzelis[13], R.L. Coxe[9], M. Cuffiani[2], S. Dado[22], G.M. Dallavalle[2], R. Davis[30], S. De Jong[12], A. de Roeck[8], P. Dervan[15], K. Desch[27], B. Dienes[32,h], M.S. Dixit[7], J. Dubbert[33], E. Duchovni[26], G. Duckeck[33], I.P. Duerdoth[16], P.G. Estabrooks[6], E. Etzion[23], F. Fabbri[2], A. Fanfani[2], M. Fanti[2], A.A. Faust[30], L. Feld[10], F. Fiedler[27], M. Fierro[2], I. Fleck[10], A. Frey[8], A. Fürtjes[8], D.I. Futyan[16], P. Gagnon[7], J.W. Gary[4], J. Gascon[18], G. Gaycken[27], C. Geich-Gimbel[3], G. Giacomelli[2], P. Giacomelli[2], V. Gibson[5], W.R. Gibson[13], D.M. Gingrich[30,a], D. Glenzinski[9], J. Goldberg[22], W. Gorn[4], C. Grandi[2], K. Graham[28], E. Gross[26], J. Grunhaus[23], M. Gruwé[27], C. Hajdu[31] G.G. Hanson[12], M. Hansroul[8], M. Hapke[13], K. Harder[27], A. Harel[22], C.K. Hargrove[7], M. Harin-Dirac[4], M. Hauschild[8], C.M. Hawkes[1], R. Hawkings[27], R.J. Hemingway[6], G. Herten[10], R.D. Heuer[27], M.D. Hildreth[8], J.C. Hill[5], P.R. Hobson[25], A. Hocker[9], K. Hoffman[8], R.J. Homer[1], A.K. Honma[28,a], D. Horváth[31,c], K.R. Hossain[30], R. Howard[29], P. Hüntemeyer[27], P. Igo-Kemenes[11], D.C. Imrie[25], K. Ishii[24], F.R. Jacob[20], A. Jawahery[17], H. Jeremie[18], M. Jimack[1], C.R. Jones[5], P. Jovanovic[1], T.R. Junk[6], N. Kanaya[24], J. Kanzaki[24], D. Karlen[6], V. Kartvelishvili[16], K. Kawagoe[24], T. Kawamoto[24], P.I. Kayal[30], R.K. Keeler[28], R.G. Kellogg[17], B.W. Kennedy[20], D.H. Kim[19], A. Klier[26], T. Kobayashi[24], M. Kobel[3,d], T.P. Kokott[3], M. Kolrep[10], S. Komamiya[24], R.V. Kowalewski[28], T. Kress[4], P. Krieger[6], J. von Krogh[11], T. Kuhl[3], P. Kyberd[13], G.D. Lafferty[16], H. Landsman[22], D. Lanske[14], J. Lauber[15], I. Lawson[28], J.G. Layter[4], D. Lellouch[26], J. Letts[12], L. Levinson[26], R. Liebisch[11], B. List[8], C. Littlewood[5], A.W. Lloyd[1], S.L. Lloyd[13], F.K. Loebinger[16], G.D. Long[28], M.J. Losty[7], J. Lu[29], J. Ludwig[10], D. Liu[12], A. Macchiolo[18], A. Macpherson[30], W. Mader[3], M. Mannelli[8], S. Marcellini[2], A.J. Martin[13], J.P. Martin[18], G. Martinez[17], T. Mashimo[24], P. Mättig[26], W.J. McDonald[30], J. McKenna[29], E.A. Mckigney[15], T.J. McMahon[1], R.A. McPherson[28], F. Meijers[8], P. Mendez-Lorenzo[33], F.S. Merritt[9], H. Mes[7], A. Michelini[2], S. Mihara[24], G. Mikenberg[26], D.J. Miller[15], W. Mohr[10], A. Montanari[2], T. Mori[24], K. Nagai[8], I. Nakamura[24], H.A. Neal[12,g], R. Nisius[8], S.W. O'Neale[1], F.G. Oakham[7], F. Odorici[2], H.O. Ogren[12], A. Okpara[11], M.J. Oreglia[9], S. Orito[24], G. Pásztor[31], J.R. Pater[16], G.N. Patrick[20], J. Patt[10], R. Perez-Ochoa[8], S. Petzold[27], P. Pfeifenschneider[14], J.E. Pilcher[9], J. Pinfold[30], D.E. Plane[8], P. Poffenberger[28], B. Poli[2], J. Polok[8], M. Przybycień[8,e], A. Quadt[8], C. Rembser[8], H. Rick[8], S. Robertson[28], S.A. Robins[22], N. Rodning[30], J.M. Roney[28], S. Rosati[3], K. Roscoe[16], A.M. Rossi[2], Y. Rozen[22], K. Runge[10], O. Runolfsson[8], D.R. Rust[12], K. Sachs[10], T. Saeki[24], O. Sahr[33], W.M. Sang[25], E.K.G. Sarkisyan[23], C. Sbarra[29], A.D. Schaile[33], O. Schaile[33], P. Scharff-Hansen[8], J. Schieck[11], S. Schmitt[11], A. Schöning[8], M. Schröder[8], M. Schumacher[3], C. Schwick[8], W.G. Scott[20], R. Seuster[14], T.G. Shears[8], B.C. Shen[4], C.H. Shepherd-Themistocleous[5], P. Sherwood[15], G.P. Siroli[2], A. Sittler[27], A. Skuja[17], A.M. Smith[8], G.A. Snow[17], R. Sobie[28], S. Söldner-Rembold[10,f], S. Spagnolo[20], M. Sproston[20], A. Stahl[3], K. Stephens[16], J. Steuerer[27], K. Stoll[10], D. Strom[19], R. Ströhmer[33], B. Surrow[8], S.D. Talbot[1], P. Taras[18], S. Tarem[22], R. Teuscher[9], M. Thiergen[10], J. Thomas[15],

M.A. Thomson[8], E. Torrence[8], S. Towers[6], I. Trigger[18], Z. Trócsányi[32], E. Tsur[23], M.F. Turner-Watson[1], I. Ueda[24], R. Van Kooten[12], P. Vannerem[10], M. Verzocchi[8], H. Voss[3], F. Wäckerle[10], A. Wagner[27], C.P. Ward[5], D.R. Ward[5], P.M. Watkins[1], A.T. Watson[1], N.K. Watson[1], P.S. Wells[8], N. Wermes[3], D. Wetterling[11] J.S. White[6], G.W. Wilson[16], J.A. Wilson[1], T.R. Wyatt[16], S. Yamashita[24], V. Zacek[18], D. Zer-Zion[8]

[1]School of Physics and Astronomy, University of Birmingham, Birmingham B15 2TT, UK
[2]Dipartimento di Fisica dell' Università di Bologna and INFN, I-40126 Bologna, Italy
[3]Physikalisches Institut, Universität Bonn, D-53115 Bonn, Germany
[4]Department of Physics, University of California, Riverside CA 92521, USA
[5]Cavendish Laboratory, Cambridge CB3 0HE, UK
[6]Ottawa-Carleton Institute for Physics, Department of Physics, Carleton University, Ottawa, Ontario K1S 5B6, Canada
[7]Centre for Research in Particle Physics, Carleton University, Ottawa, Ontario K1S 5B6, Canada
[8]CERN, European Organisation for Particle Physics, CH-1211 Geneva 23, Switzerland
[9]Enrico Fermi Institute and Department of Physics, University of Chicago, Chicago IL 60637, USA
[10]Fakultät für Physik, Albert Ludwigs Universität, D-79104 Freiburg, Germany
[11]Physikalisches Institut, Universität Heidelberg, D-69120 Heidelberg, Germany
[12]Indiana University, Department of Physics, Swain Hall West 117, Bloomington IN 47405, USA
[13]Queen Mary and Westfield College, University of London, London E1 4NS, UK
[14]Technische Hochschule Aachen, III Physikalisches Institut, Sommerfeldstrasse 26-28, D-52056 Aachen, Germany
[15]University College London, London WC1E 6BT, UK
[16]Department of Physics, Schuster Laboratory, The University, Manchester M13 9PL, UK
[17]Department of Physics, University of Maryland, College Park, MD 20742, USA
[18]Laboratoire de Physique Nucléaire, Université de Montréal, Montréal, Quebec H3C 3J7, Canada
[19]University of Oregon, Department of Physics, Eugene OR 97403, USA
[20]CLRC Rutherford Appleton Laboratory, Chilton, Didcot, Oxfordshire OX11 0QX, UK
[22]Department of Physics, Technion-Israel Institute of Technology, Haifa 32000, Israel
[23]Department of Physics and Astronomy, Tel Aviv University, Tel Aviv 69978, Israel
[24]International Centre for Elementary Particle Physics and Department of Physics, University of Tokyo, Tokyo 113-0033, and Kobe University, Kobe 657-8501, Japan
[25]Institute of Physical and Environmental Sciences, Brunel University, Uxbridge, Middlesex UB8 3PH, UK
[26]Particle Physics Department, Weizmann Institute of Science, Rehovot 76100, Israel
[27]Universität Hamburg/DESY, II Institut für Experimental Physik, Notkestrasse 85, D-22607 Hamburg, Germany
[28]University of Victoria, Department of Physics, P O Box 3055, Victoria BC V8W 3P6, Canada
[29]University of British Columbia, Department of Physics, Vancouver BC V6T 1Z1, Canada
[30]University of Alberta, Department of Physics, Edmonton AB T6G 2J1, Canada
[31]Research Institute for Particle and Nuclear Physics, H-1525 Budapest, P O Box 49, Hungary
[32]Institute of Nuclear Research, H-4001 Debrecen, P O Box 51, Hungary

[33]Ludwigs-Maximilians-Universität München, Sektion Physik, Am Coulombwall 1, D-85748 Garching, Germany

[a] and at TRIUMF, Vancouver, Canada V6T 2A3
[b] and Royal Society University Research Fellow
[c] and Institute of Nuclear Research, Debrecen, Hungary
[d] on leave of absence from the University of Freiburg
[e] and University of Mining and Metallurgy, Cracow
[f] and Heisenberg Fellow
[g] now at Yale University, Dept of Physics, New Haven, USA
[h] and Depart of Experimental Physics, Lajos Kossuth University, Debrecen, Hungary.

1 Introduction

Very little is known about the role of spin in the hadronization process. At LEP, this can be investigated by studying the properties of vector mesons produced in hadronic Z^0 decays. Recent data on the helicity states of vector mesons produced in hadronic Z^0 decays [1–4] reveal that the spin of high-energy $K^*(892)^0$ and $\phi(1020)$ mesons is preferentially aligned transverse to the direction of their momentum. Measurements of the $\rho(770)^0$ and $D^*(2010)^\pm$ mesons are consistent with this behaviour, while B^* mesons show no alignment. The mechanism at the origin of spin alignment is not well understood theoretically [5], and this phenomenon is ignored in models such as the Lund string model [6] and the cluster model [7]. Extending these studies to other vector mesons would provide valuable help in elucidating the role of spin in hadronization. The helicity density matrix elements for the $\rho(770)^\pm$ and $\omega(782)$ mesons produced in Z^0 decays have never been measured: these are particularly interesting because the most pronounced alignments observed so far are for light mesons. The $\rho^\pm$ and ω mesons, together with the ρ^0 whose helicity matrix element has already been measured [2], have a similar quark structure and can be expected to have similar behaviour. Experimentally, the systematic uncertainties affecting the extraction of the helicity matrix elements for these three mesons differ substantially.

This paper describes the measurement of the helicity density matrix elements ρ_{00} of $\rho^\pm$ and ω mesons produced in Z^0 decays using the OPAL detector at LEP. The detector and its performance are described in detail in Refs. [8–10]. The data sample consists of 4.1 million hadronic Z^0 decays collected at centre-of-mass energies within ± 2 GeV of the Z^0 peak. The selection of hadronic events is presented in Ref. [11]. The method to reconstruct and identify the $\rho^\pm \to \pi^\pm\pi^0$ and $\omega \to \pi^+\pi^-\pi^0$ decays is the same as used in Ref. [12], where it is explained in detail. The measurements of ρ_{00} for the $\rho^\pm$ and ω mesons are presented in Sections 2 and 3, and the results are compared to those for other mesons at LEP in Section 4.

2 Helicity density matrix element ρ_{00} of $\rho^\pm$ mesons

The $\rho^\pm$ resonance decays dominantly via the $\pi^\pm\pi^0$ channel. Using as a spin analyser the angle in the $\pi^\pm\pi^0$ rest frame between one of the pion momenta and the $\rho^\pm$ boost direction, the distribution of this angle, θ_H, is [13]:

$$W(\cos\theta_H) \;=\; \frac{3}{4}[(1-\rho_{00}) + (3\rho_{00}-1)\cos^2\theta_H] \qquad (1)$$

where ρ_{00} is the helicity density matrix element expressing the probability that the spin of the $\rho^\pm$ meson be perpendicular to its momentum direction.

As the mechanisms producing the observed mesons and their amount of spin alignment can vary with their energy, the analysis is repeated for different intervals of the scaled energy $x_E = E_{\rm meson}/E_{\rm beam}$.

2.1 $\rho^{\pm}$ meson reconstruction

The reconstruction of the decay $\rho^{\pm} \to \pi^{\pm}\pi^0$ follows exactly that described in Ref. [12]. Charged pion candidates are selected as tracks in the central drift chambers with an energy loss measurement having a probability greater than 1% for the pion hypothesis [10]. Neutral pions are obtained from the combination of pairs of photons detected either as localised energy deposits in the electromagnetic calorimeter or as two tracks from a $\gamma \to e^+e^-$ conversion within the volume of the central drift chambers, and selected using the multivariate method described in Ref. [12].

All selected π^0 and $\pi^{\pm}$ candidates are combined in pairs. From the energy and momenta of the π^0 and $\pi^{\pm}$ in each pair, three quantities are evaluated: the scaled energy of the pair, x_E, the invariant mass of the $\pi^{\pm}\pi^0$ system, m, and the cosine of the spin analyser angle θ_H, defined as the angle in the $\pi^{\pm}\pi^0$ rest frame between the π^0 momentum and the boost of the $\pi^{\pm}\pi^0$ system. The sample is divided into ten equal bins of $\cos\theta_H$ in the range from -1 to $+1$, for six intervals of x_E in the range from 0.025 to 1. The size of the bins in x_E and $\cos\theta_H$ are large compared to the experimental resolutions on these quantities, which are dominated by the π^0 energy resolution. The Monte Carlo simulations provide realistic estimates of these resolutions as they reproduce well the width of the π^0 mass peak [12]. They predict that the π^0 energy resolution varies between 4% and 8% over the energy range relevant for the present analysis, resulting in a resolution of approximately 0.04 on $\cos\theta_H$.

The number of reconstructed $\rho^{\pm}$ mesons in each $\cos\theta_H$ bin and x_E interval is obtained from a fit to the corresponding invariant mass distribution using the method described in Ref. [12]. These numbers are corrected by the efficiency evaluated by applying the same reconstruction method and fit procedure to a sample of 6.4 million hadronic Z^0 decays simulated [14] using the Monte Carlo programs JETSET 7.3 and 7.4 [6] tuned to reproduce the global features of hadronic events as observed by OPAL [15, 16].

Examples of invariant mass distributions and fit results are shown in Figs. 1 and 2. As can be seen, the shapes of the $\rho^{\pm}$ signal and of the underlying background vary significantly as a function of x_E and $\cos\theta_H$. According to the Monte Carlo simulations, this is due in large part to the dependence of the π^0 reconstruction efficiency on its energy. To track these effects carefully the fit procedure, described in Ref. [12] and summarised below, is applied independently to each mass distribution.

In the fit, the $\rho^{\pm}$ signal is parameterized as a relativistic Breit-Wigner convoluted with the experimental mass resolution and multiplied by a factor $1 + C\frac{m_0^2 - m^2}{m\Gamma}$ where Γ is the width of the resonance [17] and m_0 is the Breit-Wigner pole mass. This factor has been shown to take adequately into account shape distortions due to interferences and residual Bose-Einstein correlations [18]. The systematic variations of the signal shape consist of fixing C to zero or leaving it as a free parameter and, in addition, the mass resolution is set to the Monte Carlo prediction or left as a free parameter. The systematics associated with the background are evaluated using two methods. In the first, the background shape is taken from the simulation and normalised to the number of counts outside the signal region. In the second method, the background is parameterized as:

$$f(m) \;=\; p_1(m - m_{th})^{p_2} \times \exp(p_3(m - m_{th}) + p_4(m - m_{th})^2) \;, \qquad (2)$$

where $m_{th} = m_{\pi^\pm} + m_{\pi^0}$ and the parameters p_1 to p_4 are determined in the fits to the data. A Gaussian representing the reflection from $\omega \to \pi^+\pi^-\pi^0$ decays is added to this shape. Its width is fixed to the Monte Carlo prediction while its amplitude and centroid are left as free parameters in order to absorb possible imperfections in the modelling of the background near the $\pi^\pm\pi^0$ threshold. The π^0 selection is also varied as in Ref. [12], testing the sensitivity of the results to an increase and a decrease of the acceptance by a factor 2.

2.2 Extraction of the matrix element ρ_{00} of $\rho^\pm$ mesons

For each interval of x_E, the efficiency-corrected $\rho^\pm$ yields are evaluated for all ten $\cos\theta_H$ bins and fitted to the expression

$$I(\cos\theta_H) \;=\; A(1 + B\cos^2\theta_H) \;\;, \tag{3}$$

From which the value of ρ_{00} is obtained via:

$$\rho_{00} \;=\; \frac{1+B}{3+B} \;\;. \tag{4}$$

The parameters A and B and their errors are obtained from a linear least-squares fit. As an example, Fig. 3 shows the fits to the data of Figs. 1 and 2. The fit of Eqn. 3 to the data is repeated for all systematic variations of the signal and background parameterization, of the π^0 selection, and of the Monte Carlo sample used for the efficiency. The resulting B values are averaged and the systematic error associated to each source of uncertainty is taken from the rms deviation from the average. In this way, these errors reflect the uncertainty on B and are independent of global variations which affect only the parameter A.

The measured ρ_{00} values are listed in Table 1, together with the statistical errors and the errors from the following systematic uncertainties:

1. The statistical error on the Monte Carlo samples used to calculate the efficiency.
2. The bias induced by the presence of the background under the signal peak. This is estimated by the difference of the results of fits to the invariant mass spectra of Monte Carlo samples where the background is included or excluded.
3. The variations of the fitted yields when the parameterization of the shape of the signal and the background is varied as in Ref. [12].
4. The difference in efficiency obtained with Monte Carlo samples using the JETSET tune parameters of Refs. [15] and [16].
5. The variation observed when the analysis is repeated with different values for the cut on the π^0 selection variable [12], corresponding to changes by factors from 1/2 to 2 in the acceptance. As shown in Ref. [12], the variation of this cut induces significant changes in the shape of the background and therefore provides an additional test of the stability of the results relative to the assumptions regarding its shape.

3 Helicity density matrix element ρ_{00} of ω mesons

The decay $\omega \to \pi^+\pi^-\pi^0$ has a branching ratio of 88.8±0.7% [17]. In the rest frame of the $\pi^+\pi^-\pi^0$ system, the momenta of the three pions are in a plane. The appropriate spin analyser, θ_H, in this case is the angle between the normal to this plane and the boost direction [13], and Eqn. 1 applies here [19] also.

3.1 ω meson reconstruction

The reconstruction of the decay $\omega \to \pi^+\pi^-\pi^0$ follows exactly that described in Ref. [12]. Charged and neutral pion candidates are selected as in the $\rho^\pm$ analysis. All triplets comprising two oppositely charged pions and one neutral pion are considered. From the energy and momenta of the π^+, π^- and π^0 candidates three quantities are evaluated: the scaled energy of the triplet, x_E, the invariant mass of the $\pi^+\pi^-\pi^0$ system, m, and the cosine of the spin analyser angle, θ_H, defined above. The sign of $\cos\theta_H$ is arbitrary and only its absolute value is considered. The Monte Carlo simulations predict that the resolution on $|\cos\theta_H|$ is approximately 0.04, increasing to 0.06 for $0.3 < x_E < 0.6$. The sample is divided into six equal bins of $|\cos\theta_H|$ in the range from 0 to 1, for six intervals of x_E in the range from 0.025 to 1.

The number of reconstructed ω mesons in each $|\cos\theta_H|$ bin and x_E interval is obtained from a fit to the corresponding invariant mass distribution. Examples of invariant mass distributions and fit results are shown in Figs. 4 and 5. In these fits, the combinatorial background is parameterized as a third order polynomial, $P_3(m)$. As in Ref. [12], the ω signal, $S(m)$, is described as the superposition of two Gaussians sharing the same centroid, the ratios of the two widths and areas being determined from the simulation. According to the simulations, the position and total width of the peak does not depend on $|\cos\theta_H|$. Therefore, for each x_E interval, these two quantities are determined from a fit to the data in the total interval $0 < |\cos\theta_H| < 1$, and are subsequently fixed to these values in the fits to the six individual $|\cos\theta_H|$ bins.

3.2 Extraction of the matrix element ρ_{00} of ω mesons

The extracted ω yields are corrected by the reconstruction efficiency evaluated in a similar manner to that in the $\rho^\pm$ analysis (Section 2.2). For each interval in x_E, the efficiency-corrected ω yields are evaluated for the six $|\cos\theta_H|$ bins and fitted to Eqn. 3. As an example, Fig. 6 shows the fits to the data of Figs. 4 and 5. The shape of the background does not vary with x_E as much as in the case of the $\rho^\pm$, and here a fit to the sum of all x_E bins (Fig. 4) can be performed. This allows a high-statistics test of the fitting procedure. The measured ρ_{00} values are listed in Table 2, together with the statistical and systematic uncertainties. The systematic errors are evaluated as in Section 2.2. In the case of the ω, the systematic variation of the shape of the signal (third error in table 2) are derived from determining the width of the ω peak from the simulation instead of the data. As in Ref. [12], an additional error (the sixth in table 2) is derived from the test of whether the extracted ω signal has the expected dependence on the

matrix element of the ω decay [20],

$$\lambda_\omega \;=\; \frac{|\vec{p}^{\,*}_- \times \vec{p}^{\,*}_+|^2}{|\vec{p}^{\,*}_- \times \vec{p}^{\,*}_+|^2_{max}} \tag{5}$$

where $\vec{p}^{\,*}_\pm$ is the momentum of the $\pi^\pm$ meson in the $\pi^+\pi^-\pi^0$ rest frame. The λ_ω distribution is expected to rise linearly with λ_ω for the signal, and be flat for the combinatorial background. The data are therefore divided into six bins in λ_ω, and the two-dimensional distributions $I(m, \lambda_\omega)$ are fitted with the expression:

$$I(m, \lambda_\omega) \;=\; \frac{P_3(m) + \lambda_\omega S(m)}{\epsilon(m, \lambda_\omega)\,(1 + \lambda_\omega \delta)} \tag{6}$$

where $\epsilon(m, \lambda_\omega)$ is the acceptance of the detector determined from the combinatorial background distributions in the simulations, and δ is a free parameter in the fit, designed to account for possible deviations between the λ_ω-dependence of the acceptance in the data and in the Monte Carlo. The value of the sixth error in Table 2 is the difference between the results obtained from the fits to the $I(m, \lambda_\omega)$ and $I(m)$ distributions, where $I(m)$ is the sum of the six λ_ω bins.

4 Results and discussion

Tables 1 and 2 present the measured ρ_{00} values for the $\rho^\pm$ and ω mesons, respectively, together with their statistical, systematic and total errors. The total numbers of meson candidates are also listed, together with their statistical errors. The statistical errors are dominated by the contribution of the background under the $\rho^\pm$ and ω signals. The highest accessible x_E interval is $0.3 < x_E < 0.6$. The uncertainty on the $\rho^\pm$ and ω samples with $x_E > 0.6$ (approximately 400 ± 200 and 800 ± 400 candidates, respectively) is too large for a meaningful extraction of ρ_{00}. The systematic errors are evaluated using the method of Ref. [12]. In Tables 1 and 2, the scatter of the error values as a function of x_E for some uncertainty sources indicate that their evaluation may still be affected by statistical fluctuations. However the observed scatter is smaller than the size of the total errors and thus should not affect significantly the final results.

The measured values of ρ_{00} as a function of x_E are shown in Figs. 7a and b for the $\rho^\pm$ and ω mesons, respectively. The measurements are compatible with 1/3 (the dashed line in Figs 7a and b), corresponding to a statistical mix of helicity -1, 0 and $+1$ states. Out of ten measurements, eight are equal to 1/3 within one standard deviation, and two are within two standard deviations. In other cases where vector meson spin alignment has been observed [1–3] it appears only at meson energies above $x_E > 0.3$. Here, in the energy range $0.3 < x_E < 0.6$, the values of ρ_{00} for the $\rho^\pm$ and ω mesons are $0.373 \pm 0.035 \pm 0.038$ and $0.142 \pm 0.081 \pm 0.080$.

According to the Monte Carlo, and depending on the $\rho^\pm$ energy, up to 10% of $\rho^\pm$ originate from the sequential decays of $J^P = 0^-$ mesons into a $\rho^\pm$ ($J^P = 1^-$) and another $J^P = 0^-$ meson. The most important source of these decays is $\mathrm{D}^0 \to \rho^+\,\mathrm{K}^-$. In these decays the orbital angular momentum of the $\rho^\pm$ must be opposite to its intrinsic spin so that the $\rho^\pm$ must be in a helicity 0 state ($\rho_{00} = 1$) in the rest frame of the parent meson. The degree of alignment in the laboratory frame depends on the relative momenta of the $\rho^\pm$ and the parent 0^- meson. Simulations predict that only 60% of the alignment survives in the laboratory frame for $\rho^\pm$ mesons in the interval

$0.3 < x_E < 0.6$ and that it essentially disappears for $x_E < 0.1$. The effect of the alignment of the $\rho^{\pm}$ mesons coming from $J^P = 0^- \to 0^- + 1^-$ decays present in the JETSET 7.3 and 7.4 samples based on the parameters of Ref. [15] and [16] are almost indistinguishable, despite the inclusion of $L = 1$ mesons in the latter simulation. This prediction is shown in Fig. 7a as a dotted line. It agrees with the data. However, these small deviations from 1/3 at high x_E are comparable in size to the experimental errors. For the ω, the simulations predict that less than 5% of ω mesons in the interval $0.3 < x_E < 0.6$ come from $J^P = 0^- \to 0^- + 1^-$ decays. The expected impact on the average ω alignment, shown as a dotted line in Fig. 7b, is significantly smaller than in the $\rho^{\pm}$ case (Fig. 7a). If the contributions of the expected sources of $J^P = 0^- \to 0^- + 1^-$ decays are removed, the remaining population is still compatible with $\rho_{00} = 1/3$ over the entire x_E range.

Fig. 7c compares the $\rho^{\pm}$ and ω measurements with those for the $K^*(892)^0$ obtained by OPAL [3] and the ρ^0 by DELPHI [2]. The less precise DELPHI $K^*(892)^0$ data [2] are not shown for clarity: they are consistent with the OPAL data. The $K^*(892)^0$ data show a significant preference for ρ_{00} values above 1/3 at values of x_E above 0.3. By itself, the ρ^0 data was not sufficiently precise to conclude whether similar alignment values were also observed for light, unflavoured mesons in the corresponding x_E range.

Fig. 8 shows a compilation of ρ_{00} measurements for different mesons in different x_E ranges. Up to now, the B^* meson was the only case where ρ_{00}=1/3 was clearly preferred. The $K^*(892)^0$ and ϕ mesons[1] appeared to prefer larger values of $\rho_{00} > 1/2$ at high x_E, with the D^* mesons in between. In contrast, the new results on the $\rho^{\pm}$ and ω, together with the previous DELPHI ρ^0 results, appear to prefer ρ_{00} values close to 1/3. Therefore the presence of spin alignment above $x_E > 0.3$ cannot be considered to be a general property of mesons produced in hadronic Z^0 decays. This could either be due to the influence of cascade decays on the observed alignments or to some unknown mechanism producing the alignment. More measurements above $x_E = 0.3$, and particularly above 0.6, would contribute significantly to the understanding of meson spin alignment.

5 Conclusion

The helicity density matrix elements ρ_{00} of $\rho^{\pm}$ and ω mesons produced in Z^0 decays have been measured using the OPAL detector at LEP. Over the entire energy range, the measured values are compatible with 1/3 corresponding to a statistical mix of helicity -1, 0 and $+1$ states. The measurements in the highest accessible energy range $0.3 < x_E < 0.6$ are 0.373 ± 0.052 and 0.142 ± 0.114 for $\rho^{\pm}$ and ω mesons, respectively. Taken together, these results are lower than the values observed at high x_E for the $K^*(892)^0$ and ϕ mesons.

[1]The OPAL ϕ data [3] are corrected for the effects of $J^P = 0^- \to 0^- + 1^-$ decays predicted by the Monte Carlo simulations. However the size of the correction is small compared to the observed alignment.

Acknowledgements:

We particularly wish to thank the SL Division for the efficient operation of the LEP accelerator at all energies and for their continuing close cooperation with our experimental group. We thank our colleagues from CEA, DAPNIA/SPP, CE-Saclay for their efforts over the years on the time-of-flight and trigger systems which we continue to use. In addition to the support staff at our own institutions we are pleased to acknowledge the
Department of Energy, USA,
National Science Foundation, USA,
Particle Physics and Astronomy Research Council, UK,
Natural Sciences and Engineering Research Council, Canada,
Israel Science Foundation, administered by the Israel Academy of Science and Humanities,
Minerva Gesellschaft,
Benoziyo Center for High Energy Physics,
Japanese Ministry of Education, Science and Culture (the Monbusho) and a grant under the Monbusho International Science Research Program,
Japanese Society for the Promotion of Science (JSPS),
German Israeli Bi-national Science Foundation (GIF),
Bundesministerium für Bildung, Wissenschaft, Forschung und Technologie, Germany,
National Research Council of Canada,
Research Corporation, USA,
Hungarian Foundation for Scientific Research, OTKA T-029328, T023793 and OTKA F-023259.

References

[1] OPAL Collaboration, K. Ackerstaff *et al.*, Z. Phys **C 74** (1997) 437.

[2] DELPHI Collaboration, P. Abreu *et al.*, Phys. Lett. **B 406** (1997) 271.

[3] OPAL Collaboration, K. Ackerstaff *et al.*, Phys. Lett. **B 412** (1997) 210.

[4] DELPHI Collaboration, P. Abreu *et al.*, Z. Phys. **C 68** (1995) 353;
ALEPH Collaboration, D. Buskulic *et al.*, Z. Phys. **C 69** (1995) 393.

[5] J.F. Donoghue, Phys. Rev. **D 19** (1979) 2806;
J.E. Augustin and F.M. Renard, Nucl. Phys. **B 162** (1980) 341;
A.F. Falk and M.E. Peskin, Phys. Rev. **D 49** (1994) 3320;
M.A. Anselmino, M. Bertini, F. Murgia and P. Quintairos, Eur. Phys. J. C **2** (1998) 539;
and references therein.

[6] B. Andersson, G. Gustafson, G. Ingelman and T. Sjöstrand, Phys. Rep. **97** (1983) 31;
T. Sjöstrand, Comp. Phys. Comm. **39** (1986) 347;
T. Sjöstrand and M. Bengtsson, Comp. Phys. Comm. **43** (1987) 367;
T. Sjöstrand, Comp. Phys. Comm. **82** (1994) 74.

[7] B.R. Webber, Nucl. Phys. **B 238** (1984) 492.;
G. Marchesini and B.R. Webber, Nucl. Phys. **B 310** (1988) 461;
G. Marchesini *et al.*, Comp. Phys. Comm. **67** (1992) 465.

[8] OPAL Collaboration, K. Ahmet *et al.*, Nucl. Instr. and Meth. **A 305** (1991) 275.

[9] P.P. Allport *et al.*, Nucl. Instr. and Meth. **A 324** (1993) 34;
P.P. Allport *et al.*, Nucl. Instr. and Meth. **A 346** (1994) 476.

[10] M. Hauschild *et al.*, Nucl. Instr. and Meth. **A 314** (1992) 74.

[11] OPAL Collaboration, G. Alexander *et al.*, Z. Phys. **C 52** (1991) 175.

[12] OPAL Collaboration, K. Ackerstaff *et al.*, Eur. Phys. J. C **5** (1998) 411.

[13] C. Bourelly, E. Leader and J. Soffer, Phys. Rep. **59** (1980) 95.

[14] J. Allison *et al.*, Nucl. Instr. and Meth. **A 317** (1992) 47.

[15] OPAL Collaboration, M.Z. Akrawy *et al.*, Z. Phys. **C 47** (1990) 505.

[16] OPAL Collaboration, G. Alexander *et al.*, Z. Phys. **C 69** (1996) 543.

[17] The Particle Data Group, C. Caso *et al.*, Eur. Phys. J. C **3** (1998) 1.

[18] G.D. Lafferty, Z. Phys. **C 60** (1993) 659.

[19] S.M. Berman and M. Jacob, Phys. Rev. **139** (1965) B 1023.

[20] M.L. Stevenson *et al.*, Phys. Rev. **125** (1962) 687.

x_E range	Number of candidates ($\times 10^3$)	ρ_{00} value	Stat. (data)	1 Stat. (MC)	2 Bkg. bias	3 Signal shape	4 Diff. MC	5 π^0 select.	Total error
0.025 - 0.050	48 ± 5	0.312	0.066	0.004	0.000	0.000	0.005	0.047	0.081
0.050 - 0.100	156 ± 5	0.338	0.060	0.030	0.030	0.008	0.004	0.033	0.081
0.100 - 0.150	222 ± 4	0.322	0.044	0.017	0.023	0.014	0.008	0.018	0.058
0.150 - 0.300	273 ± 3	0.316	0.027	0.019	0.032	0.018	0.019	0.009	0.054
0.300 - 0.600	60 ± 1	0.373	0.035	0.029	0.001	0.011	0.009	0.022	0.052

Table 1: Measured ρ_{00} values for $\rho^{\pm}$ mesons as a function of x_E, together with the statistical, systematic and total errors. The different systematic error contributions 1–5 are described in Sect. 2.2. The total numbers of $\rho^{\pm}$ candidates in each x_E bin are also listed, together with their statistical errors, for the π^0 cut yielding the largest acceptance. These numbers are only shown to give an idea of the statistical precision of the measurement and are not used in the analysis.

x_E range	Number of candidates ($\times 10^3$)	ρ_{00} value	Stat. (data)	1 Stat. (MC)	2 Bkg. bias	3 Mass resol.	4 Diff. MC	5 π^0 select.	6 λ_ω	Total error
0.025 - 1.000	226.0 ± 2.7	0.312	0.011	0.001	0.010	0.008	0.005	0.027	0.000	0.032
0.025 - 0.050	32.8 ± 1.2	0.367	0.040	0.004	0.038	0.002	0.013	0.027	0.001	0.063
0.050 - 0.100	100.2 ± 1.7	0.249	0.018	0.003	0.047	0.008	0.008	0.038	0.007	0.065
0.100 - 0.150	47.5 ± 1.2	0.308	0.021	0.003	0.015	0.003	0.010	0.032	0.005	0.043
0.150 - 0.300	41.4 ± 1.0	0.303	0.026	0.004	0.011	0.007	0.012	0.023	0.011	0.041
0.300 - 0.600	4.8 ± 0.4	0.142	0.081	0.010	0.034	0.014	0.029	0.049	0.041	0.114

Table 2: Measured ρ_{00} values for ω mesons as a function of x_E, together with the statistical, systematic and total errors. The different systematic error contributions 1–6 are described in Sect. 2.2 and 3.2. The total numbers of ω candidates in each x_E bin are also listed, together with their statistical errors, for the π^0 cut yielding the largest acceptance. These numbers are only shown to give an idea of the statistical precision of the measurement and are not used in the analysis.

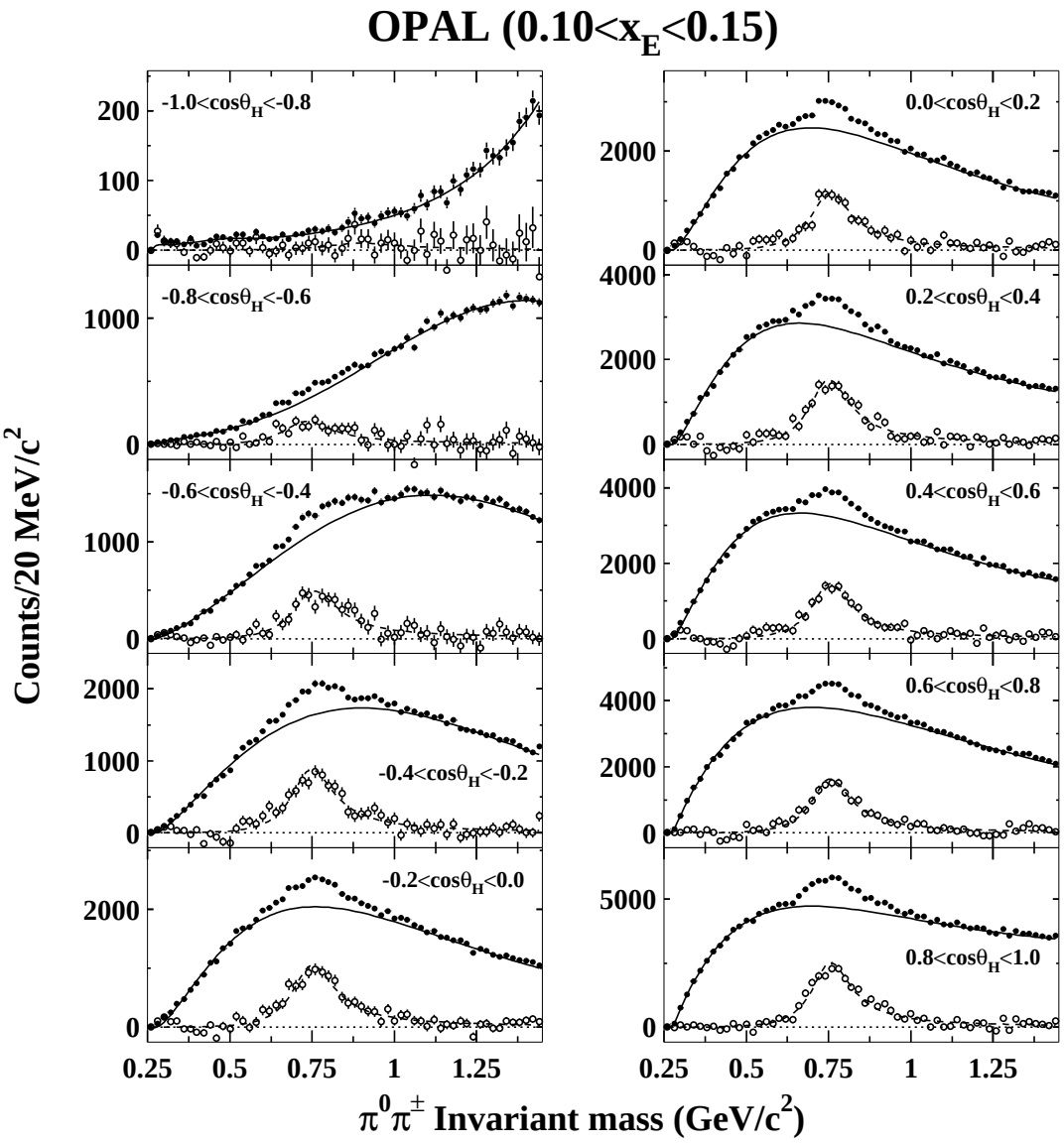

Figure 1: Invariant mass distributions of $\pi^{\pm}\pi^0$ combinations for the range $0.10 < x_E < 0.15$, for the ten equal bins of $\cos\theta_H$ between -1 and $+1$. The black circles are the data. The full lines are the background obtained in the fits to the data. The white circles show the $\rho^{\pm}$ signal, scaled by a factor 2, obtained by subtracting the fitted background (full lines) from the data. The dashed lines are the fitted signals scaled by the same factor.

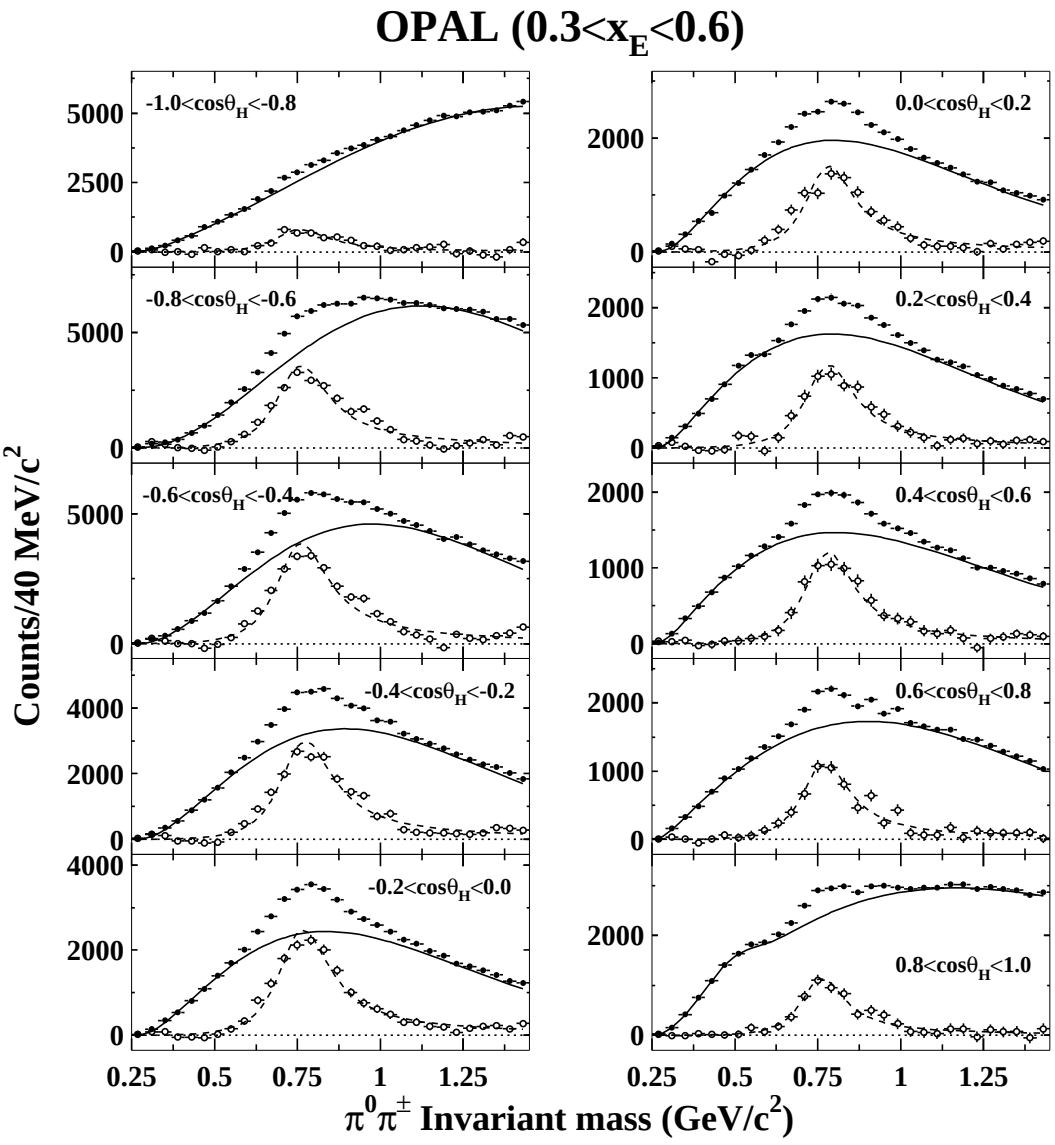

Figure 2: Invariant mass distributions of $\pi^{\pm}\pi^0$ combinations for the scaled energy range $0.3 < x_E < 0.6$, for the ten equal bins of $\cos\theta_H$ between -1 and $+1$. The black circles are the data. The full lines are the background obtained in the fits to the data. The white circles show the $\rho^{\pm}$ signal, scaled by a factor 2, obtained by subtracting the fitted background (full lines) from the data. The dashed lines are the fitted signals scaled by the same factor.

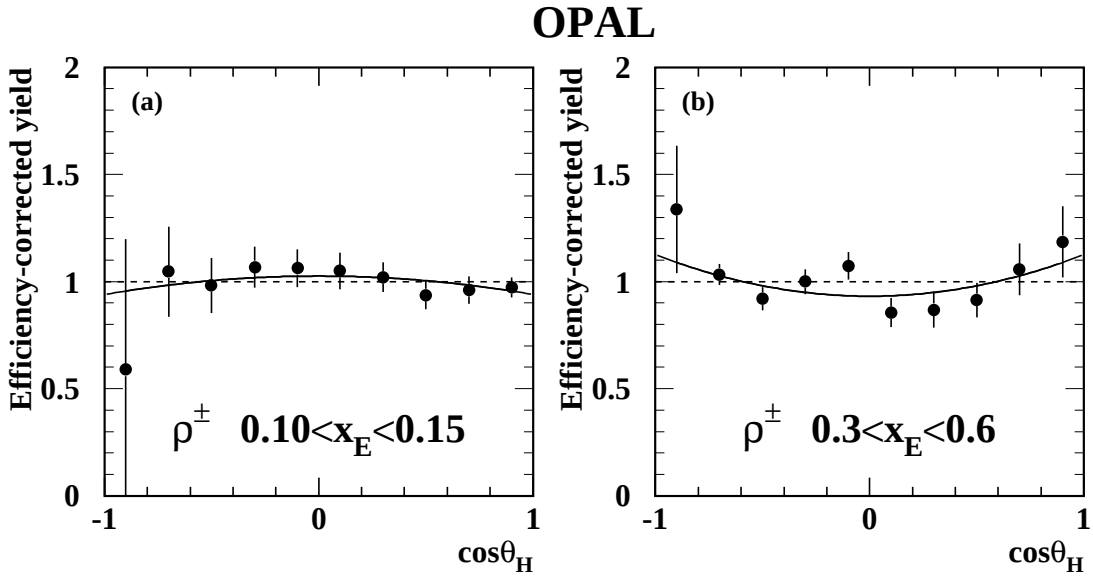

Figure 3: Efficiency-corrected $\rho^{\pm}$ yields obtained from the fits to the data shown (a) in Fig. 1 ($0.10 < x_E < 0.15$) and (b) in Fig. 2 ($0.3 < x_E < 0.6$). For clarity, the total yields are normalised to 1 using the results of the fit to the data in the entire $\cos\theta_H$ range. The errors are statistical only. The full lines represent the fit of Eqn. 3 to the data.

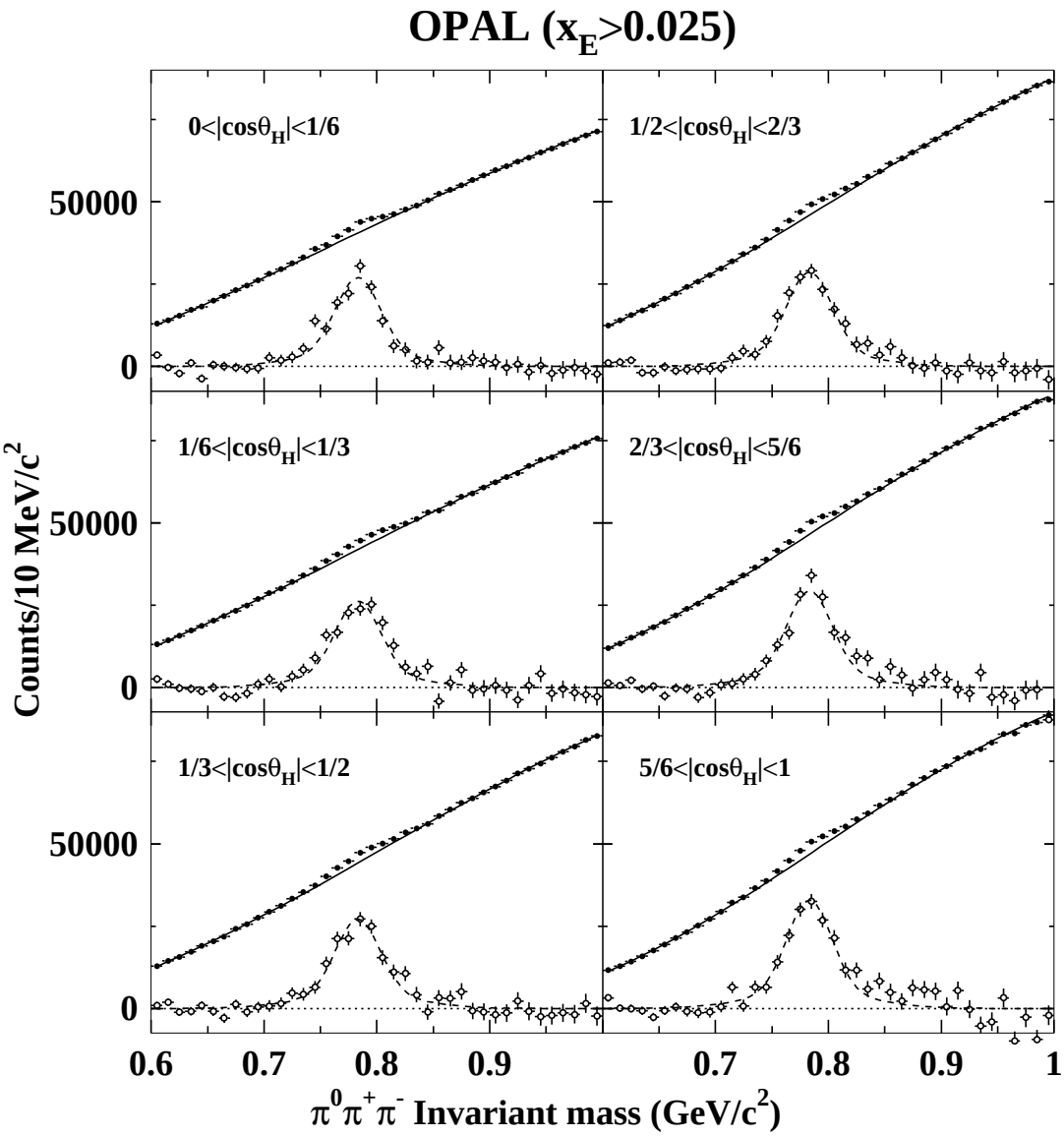

Figure 4: Invariant mass distributions of $\pi^+\pi^-\pi^0$ combinations for the range $x_E > 0.025$, for the six equal bins of $|\cos\theta_H|$ between 0 and 1. The black circles are the data. The full lines are the background obtained in the fits to the data. The white circles show the ω signal, scaled by a factor 10, obtained by subtracting the fitted background (full lines) from the data. The dashed lines are the fitted signals scaled by the same factor.

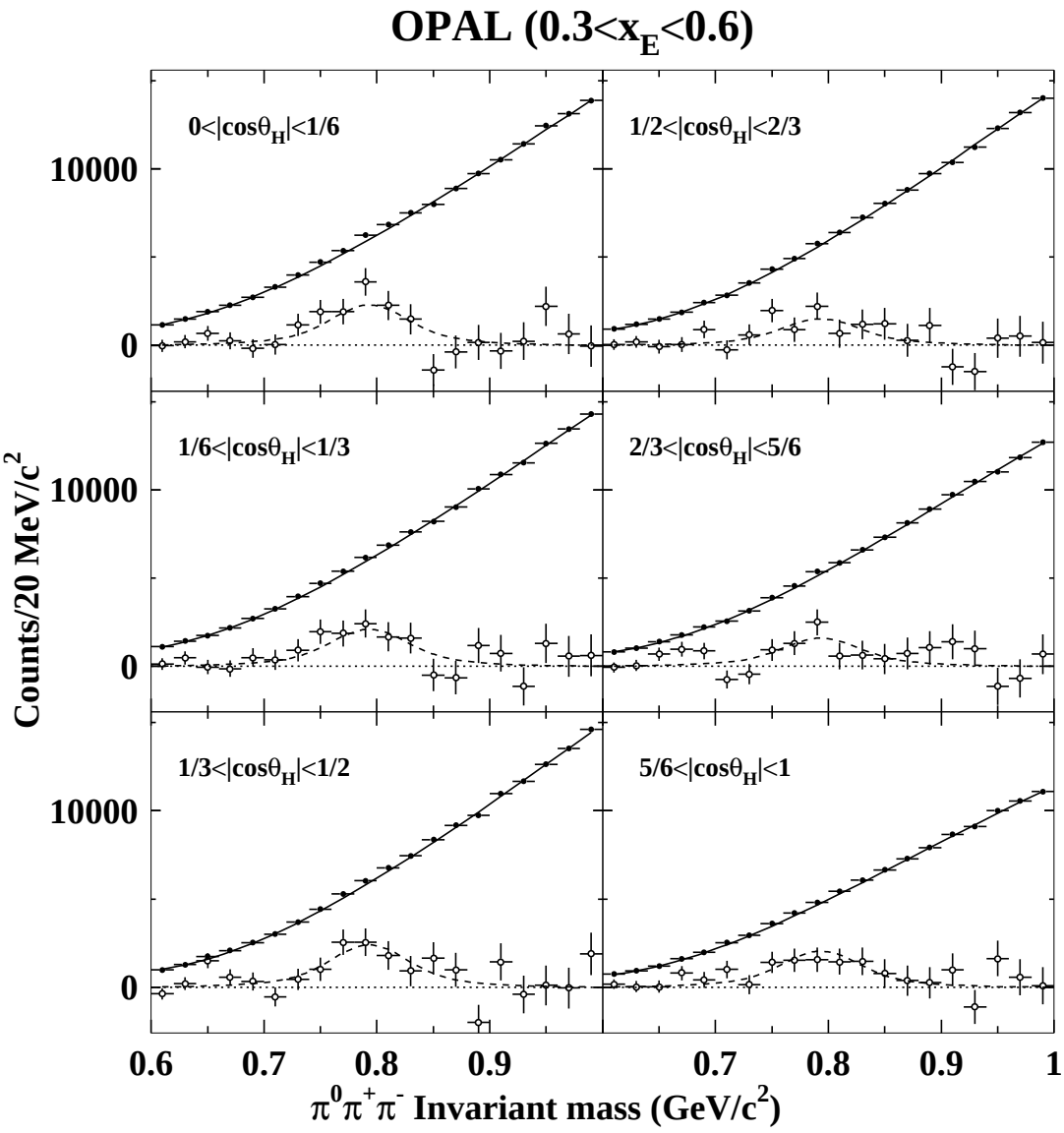

Figure 5: Invariant mass distributions of $\pi^+\pi^-\pi^0$ combinations for the scaled energy range 0.3 $< x_E <$ 0.6, for the six equal bins of $|\cos\theta_H|$ between 0 and 1. The black circles are the data. The full lines are the background obtained in the fits to the data. The white circles show the ω signal, scaled by a factor 10, obtained by subtracting the fitted background (full lines) from the data. The dashed lines are the fitted signals scaled by the same factor.

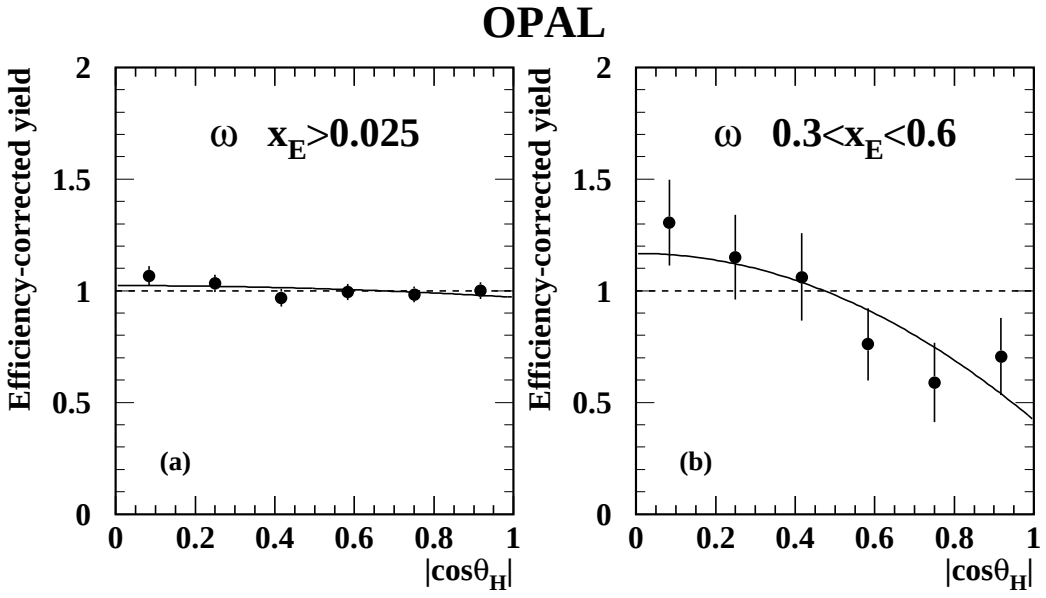

Figure 6: Efficiency-corrected ω yields obtained from the fits to the data shown (a) in Fig. 5 ($x_E > 0.025$) and (b) in Fig. 6 ($0.3 < x_E < 0.6$). For clarity, the total yields are normalised to 1 using the results of the fit to the data in the entire $|\cos\theta_H|$ range. The errors are statistical only. The full lines represent the fit of Eqn. 3 to the data.

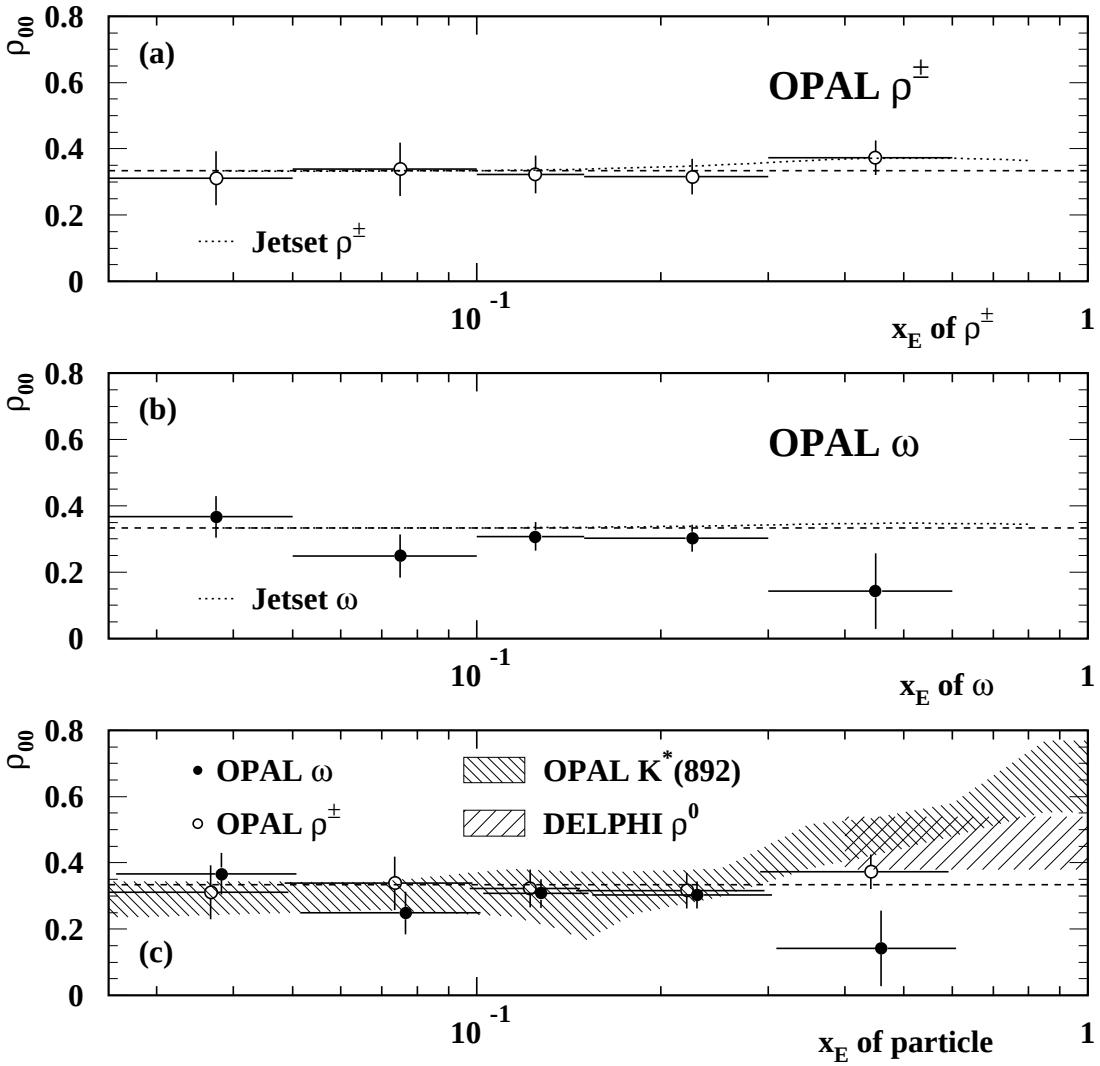

Figure 7: Measured ρ_{00} values as a function of x_E for (a) $\rho^{\pm}$ mesons and (b) ω mesons produced in Z^0 decay. The dashed lines correspond to an isotropic spin distribution (1/3). The dotted lines represent the amount of alignment expected from the $J^P = 0^- \to 0^- + 1^-$ decays present in the simulations described in Sect. 4. In (c), the data from (a) and (b) are compared with other measurements [2, 3].

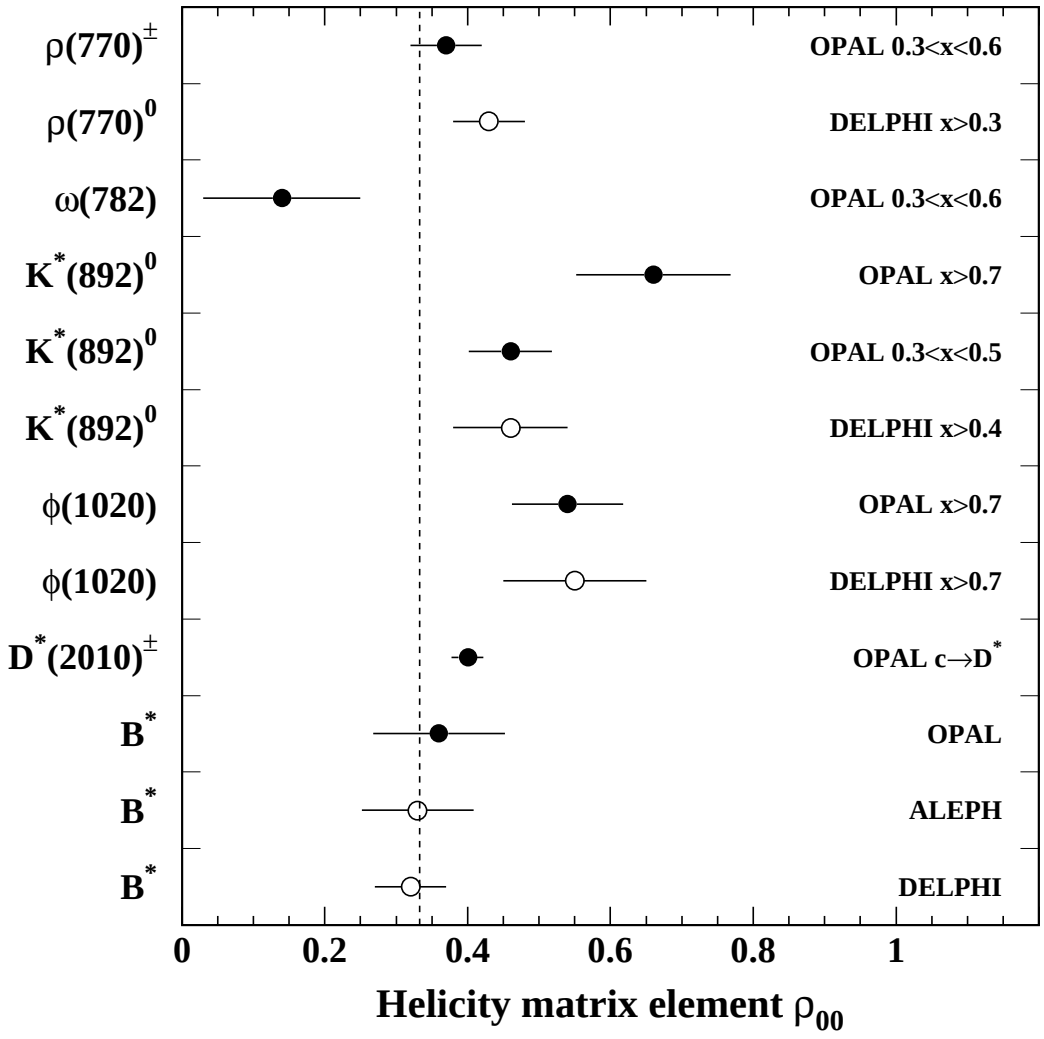

Figure 8: Summary of published ρ_{00} measurements for vector mesons produced in Z^0 decays. The results for the $\rho^{\pm}$ and ω are from this work. The Delphi results for the ρ^0, $K^*(892)^0$ and ϕ mesons are from Ref. [2], and the OPAL results for the ϕ, $D^{*\pm}$ and B^* mesons are from Ref. [1]. Other results are from Refs. [3] (OPAL $K^*(892)^0$) and [4] (ALEPH and DELPHI B^*). Only measurements at large x or corresponding to primary quarks are shown. The $K^*(892)^0$ data at $0.3 < x_E < 0.5$ and $x_E > 0.7$ are also shown as an example of the possible x_E dependence.